JACS
JOURNAL OF THE AMERICAN CHEMICAL SOCIETY
Communication
pubs.acs.org/JACS

Real-Space Distribution of Local WO_4 Ordering in Negative Thermal Expansive ZrW_2O_8

Yukio Sato,*[,†] Yasuhisa Yamamura,[‡] Kazuya Saito,[‡] and Yuichi Ikuhara[†,§]

[†]Institute of Engineering Innovation, The University of Tokyo, 2-11-16 Yayoi, Bunkyo, Tokyo 113-8656, Japan
[‡]Department of Chemistry, Faculty of Pure and Applied Sciences, University of Tsukuba, Tsukuba, Ibaraki 305-8571, Japan
[§]Nanostructures Research Laboratory, Japan Fine Ceramics Center, 2-4-1 Mutsuno, Atsuta, Nagoya 456-8587, Japan

Supporting Information

ABSTRACT: Solids usually expand when they are heated. This is quite common behavior of solids; however, there are some exceptions. Zirconium tungstate (ZrW_2O_8) is a prototype material among them, because it has the highest degree of negative thermal expansion (NTE) over broad temperature range. Intensive investigation of NTE mechanisms has suggested the importance of metal−oxygen polyhedra. However, most of the studies have been done with volume-averaged techniques, and microscopic information has been lacking. Here, our electron microscopy observations have unraveled the real-space distribution of local WO_4 tetrahedra ordering for the first time. We have found that (i) the WO_4 ordering is partly inverted; (ii) WO_4 is disordered on the nanoscale; and (iii) doping with scandium enhances the WO_4 disordering. These findings led to construction of a microstructure model for ZrW_2O_8, providing a new structural perspective for better understanding of local structure and its role in phase transitions.

Solids usually expand upon heating, having positive coefficients of thermal expansion. However, there is an exceptional class of materials that exhibit negative thermal expansion (NTE). One of the prototype materials is zirconium tungstate (ZrW_2O_8), which exhibits NTE over a broad temperature range from 4 to 1050 K.[1] This unique property of solids has attracted much attention directed toward investigating the underlying mechanism of NTE. The origin of NTE has been suggested to be, for example, low-energy phonon behavior; vibration of metal−oxygen (M−O) bonds, including libration; rigid shifting and/or rotation of M−O polyhedra; and so forth.[2−6] The discussion strongly suggests that M−O bonds and polyhedra play central roles.

The behavior of M−O polyhedra also plays an important role in the phase transition of ZrW_2O_8. Since the phase transition is accompanied by a large reduction in the cell volume, it is an important issue for NTE materials. The crystal structure of ZrW_2O_8 can be described as a combination of ZrO_6 octahedra and WO_4 tetrahedra. It undergoes a phase transition from a low-temperature phase (α; space group $P2_13$) to a high-temperature phase (β; space group $Pa\bar{3}$) at ∼440 K.[7] The α phase has a non-centrosymmetric cubic structure that can be described as a corner-sharing network of ZrO_6 octahedra and WO_4 tetrahedra[8] (Figure 1a). An O atom at one corner of each

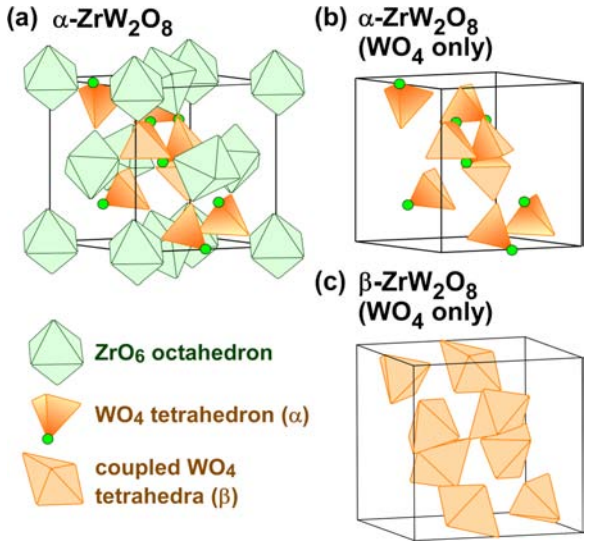

Figure 1. (a) Polyhedral representation of the crystal structure of α-ZrW_2O_8. (b) View of (a) showing only the WO_4 tetrahedra. Green circles indicate onefold-coordinated O atoms at corners of the WO_4 tetrahedra. (c) WO_4 polyhedra in the crystal structure of β-ZrW_2O_8. Here, "coupled WO_4 tetrahedra" are shown instead of WO_4 tetrahedra as in (b). W occupies two neighboring sites with 50% occupancies on average, and the change of occupation site from one to the other results in inversion of the WO_4 directions.[6] Therefore, the WO_4 direction is disordered in the β phase, which is expressed as coupled WO_4 tetrahedra.

WO_4 tetrahedron is bound only to W, resulting in its onefold coordination. The onefold-coordinated O atoms of two neighboring WO_4 tetrahedra point in the same [111] direction (Figure 1b). On the other hand, the β phase has a centrosymmetric cubic structure. Here, the onefold-coordinated O atoms of two neighboring WO_4 tetrahedra are randomly oriented in either the [111] or $[\bar{1}\bar{1}\bar{1}]$ direction (Figure 1c). Thus, WO_4 tetrahedra are ordered in the α phase and disordered in the β phase, and the degree of the ordering is linked to the α−β phase transition.

In recent years, it has been pointed out that structural inhomogeneity and the presence of nanoscale regions play important roles in a variety of physical properties.[9] Examples

Received: June 5, 2012
Published: August 16, 2012

dx.doi.org/10.1021/ja305456j | J. Am. Chem. Soc. 2012, 134, 13942−13945

include "polar nanoregions" in relaxor ferroelectrics,[10] "nanoscale phase separation" in colossal magnetoresistance oxides,[11] and so forth. The existence of nanoscale regions has been also suggested in the case of ZrW_2O_8. Yamamura et al.[12] reported that addition of a trivalent cation drastically lowers the $\alpha-\beta$ phase transition temperature, by as much as ~80 K for 4% doping with scandium (Sc). They proposed that doping with the trivalent cation forms "orientationally disordered clusters". In this model, the nanoscale clusters are understood as a statically existing β phase that is induced by Sc doping.[12]

Since most of the structural investigations of ZrW_2O_8 to date have been done with volume-averaged techniques, microstructural information for ZrW_2O_8 is not abundant. On the other hand, transmission electron microscopy (TEM) has a great potential to visualize the internal structure of materials with high spatial resolution. In addition, diffraction effects can be utilized to form TEM images, allowing us to visualize the real-space distribution of local structural characteristics. Previous TEM studies[13,14] of ZrW_2O_8 did not use this advantage efficiently and overlooked important structural characteristics at the microscopic level. In the present study, we performed TEM observations of ZrW_2O_8 in which we utilized the above advantage under careful consideration of diffraction effects. This enabled us to visualize unambiguously the real-space distribution of the local WO_4 ordering behavior in ZrW_2O_8 for the first time, leading to the construction of precise microstructure models. Sc doping effects were also clearly observed: Sc enhances the WO_4 disordering, eventually lowering the $\alpha-\beta$ phase transition temperature.

X-ray diffraction (XRD) experiments revealed that some particular reflections, such as 111, 221, and 310, appear only for the α phase;[15] these are designated as α-only reflections. The same thing basically holds for electron diffraction. Simulated diffraction patterns (DPs) from TEM of ZrW_2O_8 (Figure 2)[16] showed that the 111, 221, and 310 group reflections appear only for the α phase. This shows that the α-only reflections are characteristic of the WO_4 ordering in ZrW_2O_8. Since TEM enables an image to be formed from selected reflections in the DP [so-called dark-field (DF) TEM imaging], it was expected that information concerning WO_4 order/disorder behavior could be visualized in real space.

The contrast of each phase within the specimen was not quite clear in DF TEM images for non-α-only reflections (Figure 3a). On the contrary, DF TEM images from the same region but for an α-only reflection showed strong contrast due to the phase distribution (Figure 3b). The origin of this contrast is the breakdown of Friedel's law,[17] which is known for non-centrosymmetric crystals. The intensity of the hkl reflection becomes unequal to that for the $\overline{hkl}$ reflection in DPs for a non-centrosymmetric crystal. For α-phase ZrW_2O_8, regions (domains) with two different WO_4 ordering directions possibly exist, where the direction of onefold-coordinated O atoms is antiparallel each other. If the two different domains coexist, the hkl reflection for one domain would correspond to the $\overline{hkl}$ reflection for the other. Since the intensity of hkl is different from that for $\overline{hkl}$ because of the breakdown of Friedel's law, different domains show different contrast in DF TEM images formed from the α-only reflections characteristic of WO_4 ordering. Therefore, regions with different contrast in Figure 3b show different α-phase domains. The same trend was observed for Figure 3c, where another α-only reflection was chosen for forming the DF TEM image.

The α-phase domains were also observed for the Sc-doped specimen. The DF TEM image for an α-only reflection (Figure 3d) showed the domain-derived contrast, while that for a non-α-only reflection (Figure 3e) did not show a strong contrast variation. Comparison of the undoped and Sc-doped cases

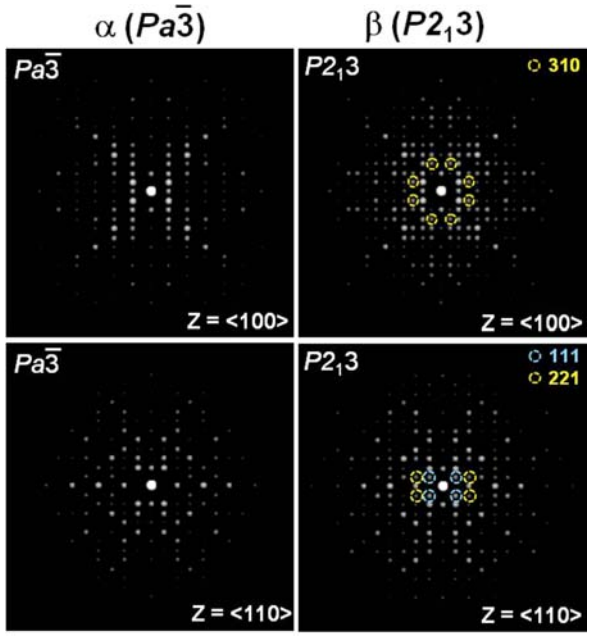

Figure 2. Simulated electron diffraction patterns for the α and β phases. DPs for incident axes $Z = \langle 100 \rangle$ and $Z = \langle 110 \rangle$ are shown, and α-only reflections such as the 111, 221, and 310 groups are indicated by circles.

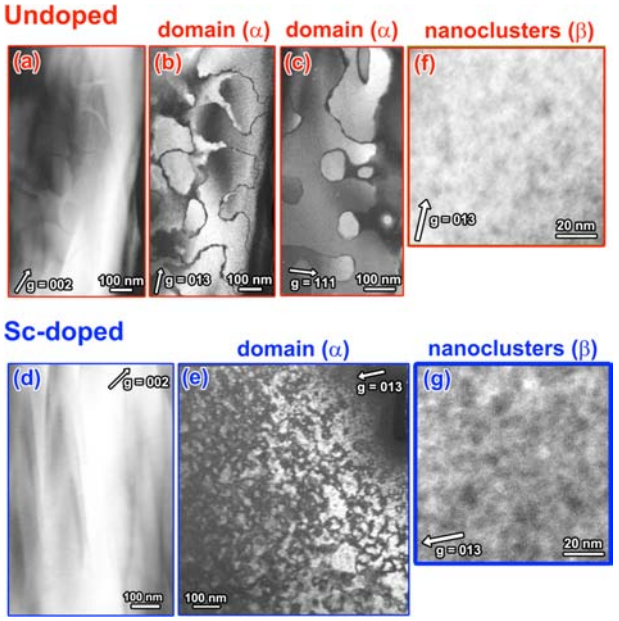

Figure 3. (a–e) DF TEM images showing α-phase domains in (a–c) undoped and (d, e) Sc-doped ZrW_2O_8. DF TEM images are shown for (a) non-α-only and (b, c) two different α-only reflections in the undoped case and for (d) non-α-only and (e) α-only reflections in the Sc-doped case. (f–g) DF TEM images showing β-phase nanoclusters. DF TEM images are shown for an α-only reflection in the (f) undoped and (g) Sc-doped cases.

dx.doi.org/10.1021/ja305456j | J. Am. Chem. Soc. 2012, 134, 13942–13945

indicates that the domain size is smaller for the Sc-doped case, implying that Sc doping tends to decrease the domain size.

Our close inspection revealed that in addition to α-phase domain contrast, dotlike dark contrast can be recognized in DF TEM images for α-only reflections (Figure 3f,g). The appearance of the dotlike contrast derives from a different imaging mechanism than for the above cases for α-phase domains. When α and β phases coexist in a region of interest in TEM, the α phase contributes to the α-only reflections while the β phase basically does not. The α-phase region would therefore be expected to look brighter and the β-phase region darker in the DF TEM image. According to this discussion, the dotlike dark contrast in Figure 3f,g is considered to be due to β-phase nanoclusters. The β-phase nanoclusters were homogeneously distributed in the specimens, and more nanoclusters were observed for the Sc-doped case. They are roughly a few nanometers in size for the undoped case (Figure 3f) and larger in size for the Sc-doped case (Figure 3g). These results clearly demonstrate that Sc doping facilitates the WO_4 disordering, leading to an increase in the β-phase volume fraction. It should also be noted here that α-phase domains and β-phase nanoclusters are statically present, since the DF TEM images were recorded by exposures of some tens of seconds. (This was also confirmed by another TEM image taken after an interval of a few minutes.)

The coexistence of the α and β phases was also revealed by direct observation of the crystal structure on the atomic scale. Figure 4a show a high-angle annular dark-field scanning TEM

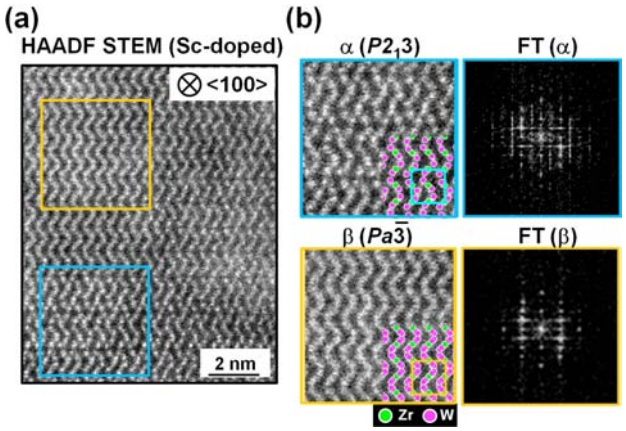

Figure 4. (a) HAADF-STEM image of Sc-doped ZrW_2O_8. The incident direction of the electrons was ⟨100⟩. (b) Magnified images of the blue and orange squares in (a). Images from (top) the α-phase region (blue) and (bottom) the β-phase region (orange) are shown with overlays of the crystal structures projected along ⟨100⟩. Zr and W columns are indicated by green and pink circles, and O columns are not visible. The blue and orange squares denote the unit cells. It should be noted here that for the β phase, the W columns with 50% occupancy[8] are also designated as green circles. This results in apparent double counting of the W columns. The Fourier transform (FT) of each region is shown alongside.

(HAADF-STEM) image of the Sc-doped specimen. The location of atomic columns can be directly observed in HAADF-STEM imaging, where the image intensity is dependent on the atomic number (Z) of the atoms included in the columns.[18] Here, the location of cation columns are observed as bright contrast, while oxygen (Z = 8) columns have weak visibility and cannot be seen. Two different phases can be directly recognized in Figure 4a. The top half is composed of the β phase. The WO_4 tetrahedra are randomly oriented, and therefore, W occupies two neighboring sites with 50% occupancy, resulting in zigzaglike contrast (orange in Figure 4b). On the other hand, the atomic arrangement differs in the bottom half of Figure 4a. Here the WO_4 tetrahedra are ordered, showing W columns as distinct spots rather than a zigzag sequence (blue in Figure 4b). This is clearly due to the presence of the α phase. The Fourier transforms (FTs) of the respective regions also support the coexistence of the α and β phases.

Thus, the present results clearly demonstrate that α-phase domains and β-phase nanoclusters coexist in ZrW_2O_8. Let us here discuss structural models in terms of the WO_4 ordering. We schematically suggest the real-space phase (WO_4 ordering) distribution for the undoped case in Figure 5 a. The material is

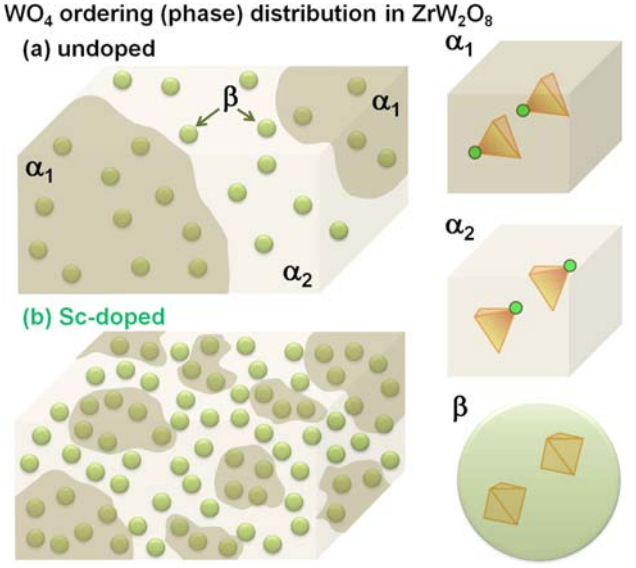

Figure 5. Schematic illustrations of the phase (WO_4 ordering) distribution in (a) undoped and (b) Sc-doped ZrW_2O_8. Different colors are used to indicate the two α-phase domains (α_1 and α_2), and small circles represent β-phase nanoclusters. At the right, the α and β phases with WO_4 tetrahedra and onefold-coordinated O atoms are shown.

divided into α-phase (α_1 and α_2) domains, and β phase nanoclusters are embedded throughout. This may look inconsistent with previous knowledge at a glance, since it has been thought from XRD results that WO_4 tetrahedra are statically fully ordered in the undoped specimen. However, existence of α-phase domains would not change the intensities of α-only reflections in powder XRD experiments, since XRD averages out hkl and $\overline{hkl}$ intensities and does not distinguish betwee hkl and $\overline{hkl}$. On the other hand, with respect to the β phase, undoped ZrW_2O_8 does not have a high density of nanoclusters. When the volume fraction is low and the size is very small, the presence of β-phase nanoclusters would not much affect the intensities of the XRD peaks. Therefore, the present results showing the existence of α-phase domains and β-phase nanoclusters in the undoped case would not be inconsistent with previous results.

It is obvious from the present results that Sc doping facilitates WO_4 disordering. The size of the α-phase domains is reduced and the density of the β-phase nanoclusters increased

dx.doi.org/10.1021/ja305456j | J. Am. Chem. Soc. 2012, 134, 13942−13945

in the Sc-doped case in comparison with the undoped case (Figure 5 b). It is therefore quite reasonable that Sc doping lowers the phase transition temperature. On the other hand, the microscopic origin of the β-phase nanoclusters is unfortunately still unclear. Point defects such as Sc at Zr sites and/or oxygen vacancies may be speculated as candidates. Since the present undoped specimen was fabricated by quenching from high temperature, oxygen vacancies may possibly be included. On the other hand, Sc doping would cause the formation of oxygen vacancies from the viewpoint of charge neutrality, and therefore, more point defects would exist for Sc-doped specimens. Thus, this scenario may account for the formation of β-phase nanoclusters in the undoped and Sc-doped specimens and the increases in cluster size and density for the Sc-doped case.

In summary, the real-space distribution of WO_4 ordering in ZrW_2O_8 has been unambiguously visualized using TEM and STEM. It has been found that the WO_4 ordering is partly inverted, forming α-phase domains, and that WO_4 is disordered in nanoscale regions, forming β-phase nanoclusters. Sc doping enhances the disordering of the WO_4 tetrahedra, drastically lowering the phase transition temperature. A new microstructure model has been suggested on the basis of these results.

■ ASSOCIATED CONTENT

Supporting Information

Experimental details. This material is available free of charge via the Internet at http://pubs.acs.org.

■ AUTHOR INFORMATION

Corresponding Author

y_sato@sigma.t.u-tokyo.ac.jp

Notes

The authors declare no competing financial interest.

■ ACKNOWLEDGMENTS

A part of this work was supported by Grants-in-Aid for Scientific Research on Priority Areas (19053001, 22015005) from the Ministry of Education, Culture, Sports, Science and Technology (MEXT), by Grants-in-Aid for Young Scientists (B) and Scientific Research (A) and (C) from the Japan Society for the Promotion of Science (JSPS), and by Nihon Sheet Glass Foundation for Materials Science and Engineering. The authors thank Ms. N. Saito for TEM specimen preparation.

■ REFERENCES

(1) Mary, T. A.; Evans, J. S. O.; Vogt, T.; Slight, A. W. *Science* **1996**, *272*, 90−92.
(2) Miller, W.; Smith, C. W.; Mackenzie, D. S.; Evans, K. E. *J. Mater. Sci.* **2009**, *44*, 5441−5451.
(3) Ernst, G.; Broholm, C.; Kowach, G. R.; Ramirez, A. P. *Nature* **1998**, *396*, 147−149.
(4) Hancock, J. N.; Turpen, C.; Schlesinger, Z.; Kowach, G. R.; Ramirez, A. P. *Phys. Rev. Lett.* **2004**, *93*, No. 225501.
(5) Tucker, M. G.; Goodwin, A. L.; Dove, M. T.; Keen, D. A.; Wells, S. A.; Evans, J. S. O. *Phys. Rev. Lett.* **2005**, *95*, No. 255501.
(6) Evans, J. S. O.; David, W. I. F.; Slight, A. W. *Acta Crystallogr., Sect. B* **1999**, *55*, 333−340.
(7) Yamamura, Y.; Tsuji, T.; Saito, K.; Sorai, M. *J. Chem. Thermodyn.* **2004**, *36*, 525−531.
(8) Evans, J. S. O.; Mary, T. A.; Vogt, T.; Subramantan, M. A.; Slight, A. W. *Chem. Mater.* **1996**, *8*, 2809−2823.
(9) Dagotto, E. *Science* **2005**, *309*, 257−262.
(10) Xu, G.; Zhong, Z.; Bing, Y.; Ye, Z.-G.; Shirane, G. *Nat. Mater.* **2006**, *5*, 134−140.
(11) Tao, J.; Niebieskikwiat, D.; Varela, M.; Luo, W.; Schofield, M. A.; Zhu, Y.; Salamon, M. B.; Zuo, J. M.; Pantelides, S. T.; Pennycook, S. J. *Phys. Rev. Lett.* **2009**, *103*, No. 097202.
(12) Yamamura, Y.; Nakajima, N.; Tsuji, T.; Kojima, A.; Kuroiwa, Y.; Sawada, A.; Aoyagi, S.; Kasatani, H. *Phys. Rev. B* **2004**, *70*, No. 104107.
(13) Xing, Q.; Xing, X.; Yu, R.; Du, L.; Meng, J.; Luo, J.; Wang, D.; Lu, G. *J. Cryst. Growth.* **2005**, *283*, 208−214.
(14) Noailles, L. D.; Peng, H.-H.; Starkovich, J.; Dunn, B. *Chem. Mater.* **2004**, *16*, 1252−1259.
(15) Allen, S.; Evans, J. S. O. *J. Mater. Chem.* **2004**, *14*, 151−156.
(16) The simulations were performed using TEMPAS software. See: Kilaas, R. *Proc—Annu. Meet., Electron Microsc. Soc. Am.* **1991**, *49*, 528−529.
(17) Miyake, S.; Uyeda, R. *Acta Crystallogr.* **1955**, *8*, 335−342.
(18) Pennycook, S. J.; Jesson, D. E. *Phys. Rev. Lett.* **1990**, *64*, 938−941.